JOURNAL OF THERMOPHYSICS AND HEAT TRANSFER
Vol. 10, No. 3, July–September 1996

# Radiative Heat Transfer Effects in Chemically Reacting Nozzle Flows

J. Liu* and S. N. Tiwari†
*Old Dominion University, Norfolk, Virginia 23529-0247*

**The two-dimensional spatially elliptic Navier–Stokes equations have been used to investigate the radiative effects in chemically reacting compressible flows of premixed hydrogen and air in an expanding nozzle. The radiative heat transfer is simulated using the Monte Carlo method. The nongray model employed is based on the statistical narrow-band model with an exponential-tailed inverse intensity distribution. The spectral correlation has been considered in the Monte Carlo formulations. Results obtained demonstrate that the radiative effects on the wall heat transfer may be significant. Extensive parametric studies are conducted to investigate the effects of equivalence ratio, wall temperature, inlet flow temperature, and the nozzle size on the radiative and convective heat fluxes on the walls.**

## Nomenclature

$A$ = reaction rate constant, also area, m$^2$
$C$ = concentration, kg-mole/m$^3$
$C_p$ = specific heat, J/(kg-K)
$D$ = diffusion coefficient, m$^2$/s
$E$ = total internal energy, J/kg, also activation energy, J/kg
$f$ = mass fraction
$g$ = Gibbs energy, J(kg-K)
$h$ = static enthalpy, J/kg
$h^R$ = base enthalpy, J/kg
$I_\omega$ = spectral radiative intensity, kW/(m$^2$-sr-cm$^{-1}$)
$k$ = thermal conductivity, J/(m-s-K), also line intensity to spacing ratio, cm$^{-1}$, atm$^{-1}$
$k_b$ = backward rate constant
$k_{eq}$ = equilibrium constant
$k_f$ = forward rate constant
$L$ = nozzle length, m
$M$ = molecular weight
$m_\omega$ = total number of narrow bands
$N$ = temperature coefficient in reaction rate expression
$N_r$ = number of reactions
$N_s$ = number of species
$p$ = gas pressure, atm
$Q$ = radiative energy per unit volume, kW/m$^3$
$q_{cw}$ = convective wall flux, kW/m$^2$
$q_{rw}$ = net radiative wall flux, kW/m$^2$
$R$ = gas constant, J/(kg-K), also random number
$R_u$ = universal gas constant, J/(kg-K)
$s$, $s'$, $s''$ = position variables, m
$T$ = absolute temperature, K
$t$ = time, s
$u$ = velocity in $x$ direction, m/s
$\tilde{u}$ = diffusion velocity in $x$ direction, m/s
$\tilde{V}$ = diffusion velocity vector, m/s
$v$ = velocity in $y$ direction, m/s
$\tilde{v}$ = diffusion velocity in $y$ direction, m/s
$\dot{w}$ = production rate of species, kg/(m$^3$-s)
$X$ = mole fraction
$x$ = $x$ coordinate, m
$y$ = $y$ coordinate, m
$y_b$ = half height of cross-sectional area of nozzle, m
$\beta$ = linewidth-to-spacing ratio
$\gamma$ = stoichiometric coefficient; also half-width of an absorption line, cm$^{-1}$
$-\nabla \cdot q_r$ = radiative source term, kW/m$^3$
$\delta$ = equivalent line spacing, cm$^{-1}$
$\theta$ = polar angle
$\mu$ = dynamic viscosity, kg/(m-s)
$\xi$, $\eta$ = computational coordinates
$\rho$ = density, kg/m$^3$
$\sigma$ = normal stress, N/m$^2$
$\tau$ = shear stress, N/m$^2$
$\tau_w$ = spectral transmittance
$\phi$ = equivalence ratio
$\psi$ = azimuthal angle
$\Omega$ = solid angle
$\omega$ = wave number, cm$^{-1}$

## Introduction

THERE has been extensive research to develop hydrogen-fueled supersonic combustion ramjet (scramjet) propulsion systems for hypersonic vehicles. One of the critical elements in the design of scramjets is the detailed understanding of the heat flux distributions on the nozzle walls for different operating conditions. Numerical simulation has been shown to be a valuable tool for gaining insight into the heat transfer on the nozzle walls.

In a hypersonic propulsion system, combustion takes place at supersonic speeds to reduce the deceleration energy loss. The products of hydrogen–air combustion are gases such as water vapor and hydroxyl radical. These species are highly radiatively participating species. This leads to the belief that the radiative energy transfer to the nozzle walls may be of significant importance in comparison to the convective heat transfer. This is quite different from the situation in the flowfield where the contribution from radiation is usually neglected in comparison to the contribution from convection or conduction.

The study of radiative transmission in nonisothermal and inhomogeneous nongray gaseous systems requires a detailed knowledge of the absorption, emission, and scattering characteristics of the specific species under investigation. In absorbing and emitting media, an accurate nongray model is of vital importance in the correct formulation of the radiative flux equations. The line-by-line models are theoretically the most precise models to treat radiative heat transfer. Solutions of the line-by-line formulation require considerably large computa-

Received May 5, 1995; revision received Feb. 4, 1996; accepted for publication Feb. 12, 1996. 

*Graduate Research Assistant, Department of Mechanical Engineering.

†Eminent Professor, Department of Mechanical Engineering.

tional resources. Currently, it is not practical to apply the line-by-line models in most engineering problems. The wideband models are the simplest nongray models and are extensively used in radiative heat transfer analyses.[1,2] By far the most popular wideband model is the exponential wideband model developed by Edwards.[3] The exponential wideband model accounts for discrete absorption bands and spectral correlations resulting from the high-resolution structure. However, the spectral discretization used in this model is too wide and it does not take into account the low-resolution correlations between intensities and transmissivities.[4,5] Also, the case of partially reflecting walls cannot be correctly modeled with this approach.[3] Recently, the narrow-band models have begun to receive a lot of attention because of the strong requirement for accurate simulation of radiation. Some narrow-band models can compare favorably to the line-by-line calculations,[4,6] and they are much simpler than the line-by-line models. In addition, the narrow-band models do not have disadvantages usually encountered with the wide-band models.

Most of the existing analyses in radiative heat transfer start with the radiative transfer equation. Use of a narrow-band model in this equation results in two types of spectral correlations.[7] One is the spectral correlation between the intensity and the transmittance within the medium. Another is the spectral correlation between the reflected component of the wall radiosity and the transmittance. To investigate the first type of spectral correlation, all of the intermediate transmittances in each finite volume element of medium along the path the radiative energy travels must be calculated and stored to make a correlated calculation. To investigate the second type of spectral correlation, a series expansion of the wall radiosity is required.[8,9] Essentially, this series expansion is utilized along with a technique for closure of the series. Consideration of the history of a finite number of reflections and approximating the remaining reflections by a closure method in the radiative transfer equation complicates the mathematical formulation and increases the computer time considerably. As the geometry considered becomes complicated, exact simulation of radiative heat transfer by most existing methods becomes very difficult for the cases with reflecting walls.

The Monte Carlo method (MCM) is not directly based on the radiative transfer equation to simulate radiative heat transfer. This results in the MCM having features different from the other methods for narrow-band analysis. When the radiative energy is transmitted in the medium, the spectral correlation only occurs between the transmittances of two different segments of the same path in the statistical relationship for determining the absorption location of an energy bundle.[10] For the case with reflecting walls, Monte Carlo treatment with a narrow-band model is similar to that with a gray model, and the second type of spectral correlation occurring in other methods does not exist. If the effect of scattering is included, a new type of spectral correlation occurs in the scattering term of the radiative transfer equation. Treatment of this spectral correlation will be far more complicated than the second type of spectral correlation mentioned earlier. In such cases, it has been indicated that only MCM can account for scattering in a correlated manner.[11]

The objective of the present study is to apply the Monte Carlo formulations with a narrow-band model to investigate radiative heat transfer effects on the walls in multidimensional chemically reacting nozzle flows. This represents a significant improvement in the treatment of radiative interaction in chemically reacting flows. Studies on radiative effects in chemically reacting viscous and supersonic flows of molecular species are limited, and radiation models used have been very simple. Mani and Tiwari[12] are the first to take into account the effects of radiation in chemically reacting supersonic flows. This work has been extended to include relatively more advanced chemistry models by Tiwari et al.[13] In both of these studies, a tangent slab approximation was employed with a gray gas model. This approximation treats the gas layer as a one-dimensional slab in evaluation of the radiative flux. Obviously, it is impossible to obtain reliable quantitative predictions of radiation from this treatment. In this study, one of the most accurate nongray models available is employed and multidimensional radiative heat transfer is simulated using the MCM. This procedure provides a more accurate prediction of the radiative effects than the previous studies.

## General Formulation

### Governing Equations

The physical model considered is a supersonic flow of premixed hydrogen and air in an expanding nozzle (Fig. 1). The nozzle wall is defined, as noted, by a quadratic curve. The inlet temperatures of hydrogen and air are high so that the chemical reaction takes place in the entire flowfield. The products of hydrogen–air combustion include water vapor and hydroxyl radical. These species are highly absorbing and emitting. To compute the radiative and convective heat transfer on the walls, the flowfield in the nozzle must be determined. To simulate the flowfield accurately, all important phenomena such as chemistry, radiation, and turbulence should be taken into account. The two-dimensional nozzle flow considered is described by the Navier–Stokes and species continuity equations that take the form in the physical coordinates as[12,13]

$$\frac{\partial \boldsymbol{U}}{\partial t} + \frac{\partial \boldsymbol{E}}{\partial x} + \frac{\partial \boldsymbol{G}}{\partial y} = \boldsymbol{H} \tag{1}$$

where vectors $\boldsymbol{U}$, $\boldsymbol{F}$, $\boldsymbol{G}$, and $\boldsymbol{H}$ are represented by

$$\boldsymbol{U} = \begin{bmatrix} \rho \\ \rho u \\ \rho v \\ \rho E \\ \rho f_j \end{bmatrix} \tag{2}$$

$$\boldsymbol{F} = \begin{bmatrix} \rho u \\ \rho u^2 - \sigma_x \\ \rho uv - \tau_{yx} \\ (\rho E - \sigma_x)u - \tau_{xy}v + q_x \\ \rho f_i(u + \tilde{u}_i) \end{bmatrix} \tag{3}$$

$$\boldsymbol{G} = \begin{bmatrix} \rho v \\ \rho uv - \tau_{xy} \\ \rho v^2 - \sigma_y \\ (\rho E - \sigma_y)v - \tau_{yx}u + q_y \\ \rho f_i(v + \tilde{v}_1) \end{bmatrix} \tag{4}$$

$$\boldsymbol{H} = \begin{bmatrix} 0 \\ 0 \\ 0 \\ -\nabla \cdot q_r \\ \dot{w}_i \end{bmatrix} \tag{5}$$

The other terms appearing in vectors $\boldsymbol{F}$, $\boldsymbol{G}$, and $\boldsymbol{H}$ are defined as

$$\sigma_x = -p + \lambda\left(\frac{\partial u}{\partial x} + \frac{\partial v}{\partial y}\right) + 2\mu\frac{\partial u}{\partial x} \tag{6}$$

$$\sigma_y = -p + \lambda\left(\frac{\partial u}{\partial x} + \frac{\partial v}{\partial y}\right) + 2\mu\frac{\partial v}{\partial y} \tag{7}$$

$$\tau_{xy} = \tau_{yx} = \mu\left(\frac{\partial u}{\partial x} + \frac{\partial v}{\partial y}\right) \tag{8}$$

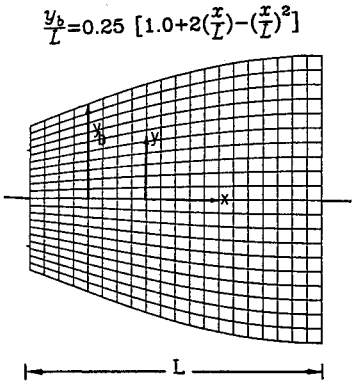


**Fig. 1 Schematic diagram of nozzle, and grid mesh for radiation simulation.**

$$q_x = -k\frac{\partial T}{\partial x} + \rho\sum_{i=1}^{N_s} h_i f_i \tilde{u}_i \tag{9}$$

$$q_y = -k\frac{\partial T}{\partial y} + \rho\sum_{i=1}^{N_s} h_i f_i \tilde{v}_i \tag{10}$$

$$E = -\frac{p}{\rho} + \frac{u^2+v^2}{2} + \sum_{i=1}^{N_s} h_i f_i \tag{11}$$

$$h_i = h_i^R + \int_{T_R}^{T} C_{p_i}\,dT \tag{12}$$

$$p = \rho T_u T \sum_{i=1}^{N_s}\frac{f_i}{M_i} \tag{13}$$

where $\lambda = -\frac{2}{3}\mu$, $\mu = \mu_l + \mu_t$, and $k = k_l + k_t$. In this study the molecular viscosity $\mu_l$ and molecular thermal conductivity $k_l$ are evaluated from Sutherland's law[14]; the turbulent viscosity $\mu_t$ is evaluated from the Baldwin–Lomax model, and the turbulent thermal conductivity $k_t$ is calculated from the turbulent Prandtl number.

In Eqs. (1), only $(N_s - 1)$ species equations need to be considered since the mass fraction of the species is prescribed by satisfying the constraint equation

$$\sum_{i=1}^{N_s} f_i = 1 \tag{14}$$

The diffusion velocity of the $i$th species is obtained by solving the Stefan–Maxwell equation,[15] neglecting the body force and thermal diffusion effects, as

$$\nabla X_i = \sum_{j=1}^{N_s}\left(\frac{X_i X_j}{D_{ij}}\right)(\tilde{V}_j - \tilde{V}_i) + (f_i - X_i)\left(\frac{\nabla p}{p}\right) \tag{15}$$

where $D_{ij} = D_{ij}^l + D_{ij}^t$. The molecular diffusion coefficient $D_{ij}^l$ is obtained from the kinetic theory[15] and the turbulent diffusion coefficient $D_{ij}^t$ is evaluated from the turbulent Schmidt number. Equation (15) has to be applied only to $(N_s - 1)$ species. The diffusion velocity for the remaining species is prescribed by satisfying the constraint equation $\sum_{i=1}^{N_s} f_i\tilde{V}_i = 0$, which ensures consistency.

Although it is well known that the radiative effects on the flowfield in supersonic flows are small, $-\nabla\cdot q_r$ is still included in the energy equation in this study and it is treated as a source term. The simulation of this source term is explained in detail later.

**Thermodynamic and Chemistry Models**

The specific heat of individual species $C_{p_i}$ is defined by a fourth-order polynomial in temperature

$$C_{p_i}/R = A_i + B_i T + C_i T^2 + D_i T^3 + E_i T^4 \tag{16}$$

The values of the coefficients appearing in Eq. (16) are found in Ref. 16. Knowing the specific heat of each species, the enthalpy of each species can be found from Eq. (12) and the total internal energy is computed from Eq. (11).

Chemical reaction rate expressions are usually determined by summing the contributions from each relevant reaction path to obtain the total rate of change of each species. Each path is governed by a law of mass action expression in which the rate constants can be determined from a temperature-dependent Arrhenius expression. In vector $\boldsymbol{H}$, the term $\dot{w}_i = M_i C_i$ represents the net rate of production of species $i$ in all chemical reactions and is modeled as follows:

$$\sum_{i=1}^{N_s}\gamma'_{ij}C_j \underset{k_{b_j}}{\overset{k_{f_j}}{\rightleftharpoons}} \sum_{i=1}^{N_s}\gamma''_{ij}C_j, \qquad j = 1,\ldots,N_r \tag{17}$$

$$\dot{w}_i = M_i C_i = M_i\sum_{j=1}^{N_r}(\gamma''_{ij} - \gamma'_{ij})\left(k_{f_j}\prod_{m=1}^{N_s} C_m^{\gamma'_{jm}} - k_{b_j}\prod_{m=1}^{N_s} C_m^{\gamma''_{jm}}\right) \tag{18}$$

Equation (17) represents the $N_r$-step chemical reaction, and Eq. (18) is the production rate for the $i$th species. The reaction constants $k_{f_j}$ and $k_{b_j}$ are calculated from the following equations:

$$k_{f_j} = A_j T^{N_j}\exp[(E_j/R_u T)], \qquad j = 1,\ldots,N_r \tag{19}$$

$$k_{b_j} = k_{f_j}/k_{eq_j}, \qquad j = 1,\ldots,N_r \tag{20}$$

The equilibrium constant appearing in Eq. (20) is given by

$$k_{eq_j} = \left(\frac{1}{R_u T}\right)^{\Delta n_j}\exp\left(\frac{-\Delta G_{R_j}}{R_u T}\right), \qquad j = 1,\ldots,N_r \tag{21}$$

where

$$\Delta n_j = \sum_{i=1}^{N_s}\gamma''_{ij} - \sum_{i=1}^{N_s}\gamma'_{ij}, \qquad j = 1,\ldots,N_r \tag{22}$$

$$\Delta G_{R_j} = \sum_{i=1}^{N_s}\gamma''_{ij}g_i - \sum_{i=1}^{N_s}\gamma'_{ij}g_i, \qquad j = 1,\ldots,N_r \tag{23}$$

$$\frac{g_i}{R_i} = A_i(T - \ell n\ T) - \frac{B_i}{2}T^2 - \frac{C_i}{6}T^3 - \frac{D_i}{12}T^4 - \frac{E_i}{20}T^5 + F_i - G_i T, \qquad i = 1,\ldots,N_r \tag{24}$$

The forward rate for each reaction is determined from Eq. (19). The hydrogen–air combustion mechanism used in this work is from Ref. 17, but only seven species and seven reactions are selected for this study. The constants $A_j$, $N_j$, and $E_j$ for these reactions are listed in Table 1. The species Gibb's

**Table 1 Hydrogen-air combustion mechanism (seven species, seven reactions)**

| No. | Reaction | $A$ | $N$ | $E$ |
|---|---|---|---|---|
| 1 | $H_2 + O_2 \rightarrow OH + OH$ | 1.70E+13 | 0.0 | 24,233 |
| 2 | $H + O_2 \rightarrow OH + O$ | 1.42E+14 | 0.0 | 8,250 |
| 3 | $OH + H_2 \rightarrow H_2O + H$ | 3.16E+07 | 1.8 | 1,525 |
| 4 | $O + H_2 \rightarrow OH + H$ | 2.07E+14 | 0.0 | 6,920 |
| 5 | $OH + OH \rightarrow H_2O + O$ | 5.50E+13 | 0.0 | 3,523 |
| 6 | $H + OH + M \rightarrow H_2O + M$ | 2.21E+22 | −2.0 | 0 |
| 7 | $H + H + M \rightarrow H_2 + M$ | 6.53E+17 | −1.0 | 0 |

free energy, Eq. (24), is obtained from the integration of the specific heat $C_{p_i}$. The coefficients in Eq. (24) are the same as in Eq. (16).

## Radiation Transfer Model

The radiative effects on the nozzle flowfield arise through the term $-\nabla \cdot q_r$ in the energy equation and the radiative effects on the heat transfer on the nozzle walls arise through the term $q_{rw}$. The expressions for both $-\nabla \cdot q_r$ and $q_{rw}$ are very complicated integrodifferential equations and they are usually treated separately from the governing equations. Before applying MCM to evaluate $-\nabla \cdot q_r$ and $q_{rw}$, temperature, concentration of species, and pressure in the media should be assumed. Next, the participating media and the surrounding walls are divided into volume elements and surface elements. In this study, the body-fitted grid mesh as shown in Fig. 1 is used for radiation simulation to obtain accurate results.

For an arbitrarily chosen volume element with a volume $\delta V$ and an arbitrarily chosen surface element with an area $\delta A$, the relations for $-\nabla \cdot q_r$ and $q_{rw}$ are expressed as[18]

$$-\nabla \cdot q_r = \frac{Q_{V-\delta V} + Q_{A-\delta V} - Q_{\delta V}}{\delta V} \tag{25}$$

$$q_{rw} = \frac{Q_{V-\delta A} + Q_{A-\delta A} - Q_{\delta A}}{\delta A} \tag{26}$$

Here, $Q_{V-\delta V}$ and $Q_{V-\delta A}$ are the total radiant energy from the entire gas that are absorbed by the volume element $\delta V$ and surface element $\delta A$, respectively; $Q_{A-\delta V}$ and $Q_{A-\delta A}$ are the total radiant energy from the bounding walls that are absorbed by $\delta V$ and $\delta A$, respectively; $Q_{\delta V}$ and $Q_{\delta V}$ are the radiant energy emitted by $\delta V$ and $\delta V$, respectively.

Evaluation of the terms $Q_{V-\delta V}$, $Q_{A-\delta V}$, $Q_{\delta V}$, and $Q_{V-\delta A}$ in Eqs. (25) and (26) requires a detailed knowledge of the absorption, emission, and scattering characteristics of the specific gas. Several models are available in the literature to represent the absorption emission characteristics of molecular species. An accurate nongray model (employed in this study) is the statistical narrow-band model with an exponential-tailed inverse intensity distribution. The transmittance predicted by this model in a homogeneous and isothermal column of length $l$ because of gas species $j$, averaged over $[\omega - (\Delta\omega/2), \omega + (\Delta\omega/2)]$, is expressed as[19]

$$\bar{\tau}_\omega^j = \exp\left\{-\frac{\bar{\beta}}{\pi}\left[\sqrt{\left(1 + \frac{2\pi X_j p l \bar{k}}{\bar{\beta}}\right)} - 1\right]\right\} \tag{27}$$

where $X_j$ represents the mole fraction of the absorbing species $j$; $\bar{k}$ and $\bar{\beta} = 2\pi\bar{\gamma}/\bar{\delta}$ are the band model parameters that account for the spectral structure of the gas. The overbar symbol indicates that the quantity is averaged over a finite wave number interval $\Delta\omega$. Parameters $\bar{k}$ and $1/\bar{\delta}$ generated from a line-by-line calculation have been published for $H_2O$, $CO_2$, CO, OH, NO, and other species.[6,20,21] The mean half-width $\bar{\gamma}$ is obtained using the parameters suggested by Soufiani et al.[6] The narrow-band width considered is usually 25 $cm^{-1}$. Nonisothermal and inhomogeneous media are treated by using the Curtis-Godson approximation.[22]

To simulate radiative heat transfer using the MCM, the total radiant energy in a volume element or surface element is assumed to be composed of many energy bundles. These energy bundles are similar to photons in their behavior. The histories of these energy bundles are traced from their point of emission to their point of absorption. What happens to each of these bundles depends on the emissive, scattering, and absorptive behavior within the medium that is described by a set of statistical relationships. The detailed discussion of the MCM has been provided by Howell.[23] However, not all of the statistical relationships given by Howell are applicable while using narrow-band models. An important change is the necessity of spectrally averaging the radiative properties within each narrow band. This results in spectrally correlated formulations. For a volume element, the total emitted radiant energy and major statistical relationships in conjunction with a narrow-band model are given by[24]

$$Q_{dV} = 4\pi \sum_{k=1}^{m_\omega} (\overline{\kappa_{\omega^k}}\,\overline{I_{b\omega^k}}\Delta\omega^k)\, dV \tag{28}$$

$$R_\omega = \frac{4\pi \sum_{k=1}^{n} (\overline{\kappa_{\omega^k}}\,\overline{I_{b\omega^k}}\Delta\omega^k)\, dV}{Q_{dV}}, \qquad (\omega^{n-1} < \omega \le \omega^n) \tag{29}$$

$$R_\theta = (1 - \cos\theta)/2 \tag{30}$$

$$R_\psi = \psi/2\pi \tag{31}$$

$$R_l = \frac{L_m}{\ell n\, \overline{\tau_\omega}(L_m)}\left(\frac{\partial \overline{\tau_\omega}}{\partial l}\right) \tag{32}$$

Here, $n$ represents the total number of narrow bands, and $\overline{\kappa_{\omega^k}}$ is the mean absorption coefficient over the $k$th narrow band and is obtained as[25]

$$\overline{\kappa_{\omega^k}} \approx \frac{\ell n\, \overline{\tau_{\omega^k}}(L_m)}{L_m} \tag{33}$$

In Eqs. (28–33), $L_m$ is the mean beam length of the volume element, $I_{b\omega^k}$ is the Planck spectral blackbody intensity for the $k$th narrow band, $\theta$ and $\psi$ are the polar and azimuthal angles of emission direction of an energy bundle, respectively, $m_\omega$ is the total number of narrow bands, and $R_\omega$, $R_\theta$, $R_\psi$, and $R_l$ are random numbers that are uniformly distributed between zero and one. The length $L_m$ is equal to the volume of an element divided by the element boundary area and then multiplied by a factor of 3.6 (Ref. 25). The statistical relationships for an energy bundle emitted from a surface element are similar to those given by Howell[23] and they are not listed here.

A large number of energy bundles is considered to satisfactorily represent the radiation emitted by a volume or surface element. The total number of energy bundles absorbed by each element multiplied by the energy per bundle gives the interchange of radiation among the volume and/or surface elements. The values of $-\nabla \cdot q_r$ and $q_{rw}$ can then be obtained from Eqs. (25) and (26), respectively. Substituting $-\nabla \cdot q_r$ into the energy equation, Eqs. (1) can be solved.

## Method of Solution

Equations (1) are written in the the physical domain $(x, y)$ and must be transformed to an appropriate computational domain $(\xi, \eta)$ for solution. Using an algebraic grid generation technique, a highly clustered grid in the physical domain (near regions where high gradients exist) can be obtained. In the computational domain, Eqs. (1) are expressed as

$$\frac{\partial \hat{U}}{\partial t} + \frac{\partial \hat{F}}{\partial \xi} + \frac{\partial \hat{G}}{\partial \eta} = \hat{H} \tag{34}$$

where

$$\hat{U} = UJ, \quad \hat{F} = Fy_\eta - Gx_\eta, \quad \hat{G} = Gx_\xi - Fy_\xi$$
$$\hat{H} = HJ, \quad J = x_\xi y_\eta - y_\xi x_\eta \tag{35}$$

Here $J$ is the Jacobian of the transformation.

The governing equation system, Eq. (34), can be stiff because of the kinetic source terms contained in the vector $\boldsymbol{H}$. To deal with the stiff system, the kinetic source terms are computed implicitly in the temporally discrete form of Eq. (34). Once the temporal discretization is performed, the resulting system is spatially differenced using the explicit, unsplit MacCormack predictor–corrector schemes. This results in a spatially and temporally discrete, simultaneous system of equations at each grid point. Each simultaneous system is solved, subject to initial and boundary conditions. At the supersonic inflow boundary, all flow quantities are specified. At the supersonic outflow boundary, nonreflective boundary conditions are used. Only the upper half of the flow domain is computed, as the flow is assumed to be symmetric about the centerline of a two-dimensional nozzle. The upper boundary is treated as a solid wall. This implies a no-slip boundary condition. The wall temperature is given and wall species mass fractions and pressure are extrapolated from interior grid points, by assuming a noncatalytic wall as well as the boundary-layer assumption on the pressure gradient. Symmetry boundary conditions are imposed at the lower boundary, that is, at the centerline. Initial conditions are obtained by specifying inlet flow conditions throughout the flowfield. The resulting set of equations is marched in time, until steady-state solutions are achieved.

With consideration of radiative heat transfer, solution procedures employed in this study are summarized next.

1) First, Eqs. (1) are solved without consideration of radiation in terms of the modified MacCormack schemes.

2) The steady solutions for temperature, pressure, and species mass fractions are then used for Monte Carlo simulation. The computed radiative source term $-\nabla \cdot q_r$ from the MCM is based on a different grid from that used for Eqs. (1). Linear interpolation and extrapolation are employed for the transformation of $-\nabla \cdot q_r$ between the two grids.

3) The transformed $-\nabla \cdot q_r$ is substituted into Eqs. (1), and equations are solved again. If the differences between two consecutive steady solutions are smaller than a designated tolerance, the computation ends. Otherwise, steps (2) and (3) are repeated until solutions converge.

Note that there are two levels of numerical procedures employed here, which result in two different iterative procedures. One is the numerical procedure for solving the Eqs. (1) and solutions iterate with time. The other is the numerical procedure for evaluating the radiative source term using the MCM, which results in the iteration of steady-state solutions.

## Results and Discussion

Based on the theoretical and numerical procedures described earlier, a computer code has been developed to simulate the two-dimensional supersonic chemically reacting and radiating nozzle flows on a Cray X-MP machine. The specific objective of this study is to investigate the radiative heat transfer to the nozzle wall. The problem considered in this study contains four parameters: 1) equivalence ratio of hydrogen and air, 2) inlet flow temperature, 3) wall temperature, and 4) nozzle size. Numerical solutions are obtained for a variety of combinations of these parameters. In each problem, flow is introduced to the nozzle at the same velocity of 1230 m/s and the same pressure of 1 atm. The grid size for solving the governing equations is $71 \times 41$ (upper half of the nozzle). Further refinement of the grid yields little changes in the results. For a given radiative source distribution, the residuals of Eqs. (1) are reduced by eight orders of magnitude in 3000 iterations for a typical case and the steady-state solutions are considered to have been obtained. The corresponding CPU time is about 6 min. To check the accuracy of a computational scheme, a preliminary calculation has been carried out for chemically reacting nozzle flows without consideration of radiation. The results from this study show very good agreement with available solutions.[26,27]

For the temperature ranges considered, the important radiating species are OH and $H_2O$. But OH is a much less radiation participating species than $H_2O$. In addition, the concentration of OH is about 10–20 times less than that of $H_2O$ for the problems considered. Therefore, the contribution of radiation from OH has been neglected. For $H_2O$, all important bands have been taken into account and they consist of 295 narrow bands in the spectral range from 150 to 7500 $cm^{-1}$ (Ref. 20). In addition, for all the cases considered, the nozzle wall is assumed to be gray and the wall emissivity is taken to be 0.8. The inlet and outlet surfaces of the nozzle flow are treated as pseudoblack walls. The temperature of the inlet surface is equal to the inlet flow temperature and determination of the temperature of the outlet surfaces is discussed later.

To assure that the statistical results make sense in the Monte Carlo simulation, two requirements must be met. One is the accuracy of statistical results for a given grid. The other is the independence of the results on a grid. In this study, the designated statistical accuracy of the results is defined in such a way that when the relative statistical errors of results are less than ±5%, the probability of the results lying within these limits is greater than 95%. Independence of the results on a grid is considered to have been achieved when the volume element number in the $x$ direction is 20 and the volume element number in the $y$ direction is 20 as shown in Fig. 1. For this grid, the total number of energy bundles had to be 2,000,000 and the required CPU time was about 1 h to meet the designated statistical accuracy in results for a typical problem.

The grid considered for Monte Carlo computations is coarser than that for numerical solutions of the energy equation. The intermediate values of the radiative source term, within the grid for solutions of Eqs. (1), are obtained by interpolation and extrapolation. This should not introduce significant errors as the radiative source term is a slowly varying function compared to the temperature and its derivative.[28] The major CPU time consumed is in the Monte Carlo simulation. It is believed that the computational time for Monte Carlo simulation could be reduced considerably if the code is vectorized and parallelized.

Figures 2a–2c show the temperature, pressure, and $H_2O$ mass fraction distributions for a typical problem in which the equivalence ratio of hydrogen and air, wall temperature, inlet flow temperature, and the nozzle length are taken to be $\phi$ = 1.0, $T_w$ = 1900 K, $T_i$ = 1900 K, and $L$ = 2.0 m, respectively. This information is essential to analyze the effects of radiative heat transfer. As the premixed mixture of hydrogen and air enters the nozzle, an exothermic chemical reaction takes place immediately, and the temperature and pressure increase abruptly and reach their peaks in a region close to the inlet location (Figs. 2a and 2b). During this rapid change in temperature and pressure, the mass fraction of $H_2O$ also experiences a big jump from zero to a value that varies little in the rest of the flow regime (Fig. 2c). As the flow continues to move downstream, supersonic expansion plays a major role, and the temperature and pressure are decreased. At the same time, the chemical reaction proceeds, but it becomes very weak. This is why there is a little change in $H_2O$ mass fraction in the downstream region. Computations have been conducted also for other cases, similar trends in results for temperature, pressure, and $H_2O$ mass fractions are observed.

In obtaining the results presented in Figs. 2a–2c, the temperature of the pesudoblack outlet surface was selected to be equal to the average temperature between the local exit gas temperature and the environment temperature (300 K). Numerical studies were conducted also for two other cases with the temperature of the outlet surface (for radiation) equal to the local exit gas temperature and the environment temperature, respectively. These two cases represent two limiting effects of radiation in the nozzle flow. It is found that no matter what outlet boundary condition for radiation is given, the radiative source term in the energy equation is usually three orders of magnitude less than the convective or conductive

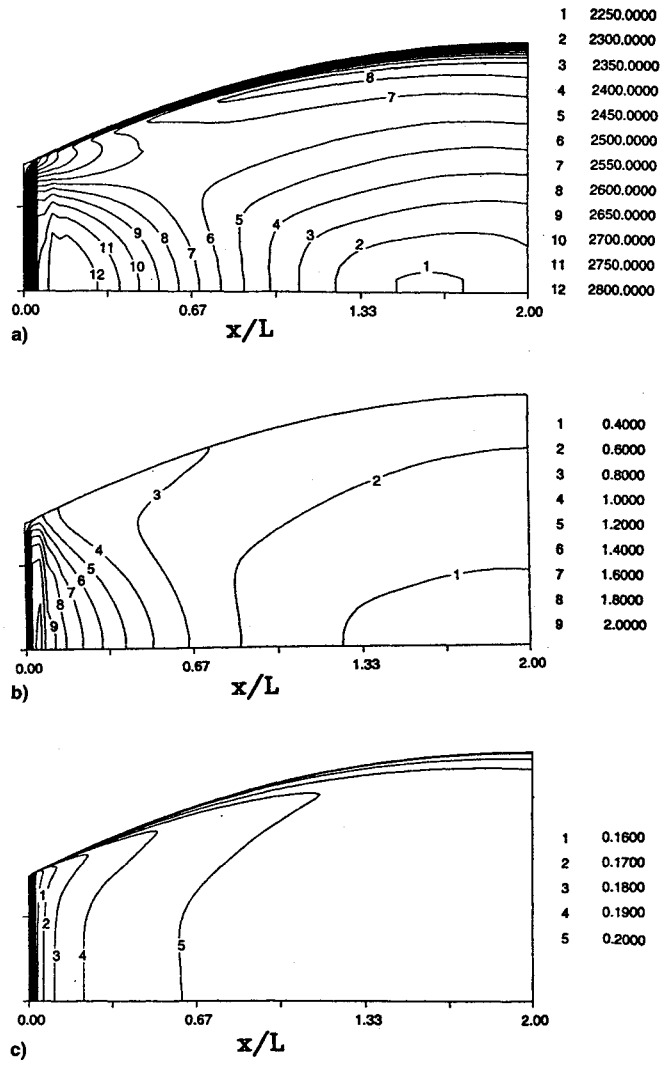


**Fig. 2 a) Temperature, b) pressure, and c) $H_2O$ mass fraction contours in the nozzle.**

term. Therefore, as expected, the radiative effects on the flowfield in supersonic flows are negligible and an iterative procedure is not necessary in the evaluation of radiation using the MCM.

The effects of three different outlet boundary conditions for radiation on the radiative wall flux distribution are shown in Fig. 3. Note that results are much higher for the case with the outlet boundary temperature equal to the local exit gas temperature. For a realistic case, however, the temperature downstream from the nozzle exit decreases rapidly because of mixing and/or expansion of the plume. Thus, the effective radiating temperature at the exit will be well below the nozzle exit temperature. Therefore, in this study, the temperature of the pesudoblack outlet wall is selected to be equal to the average temperature between the local exit gas temperature and the environment temperature.

In chemically reacting and radiating compressible flows, the radiation could be simulated by employing realistic or simplified models. Figures 4a and 4b demonstrate the differences in three different treatments of radiation. Figure 4a shows the results for the radiative source distribution at $X/L = 0.5$, and Fig. 4b presents the results for the radiative wall flux as a function of $X/L$. The physical conditions for these results are the same as for Figs. 2a–2c. The nongray treatment is the one described in this study and the results are labeled as nongray in the figures. In the second treatment, radiation transmission in the gas is simulated by the gray gas model as given in Refs. 12 and 13 and the results are labeled as gray. In the third

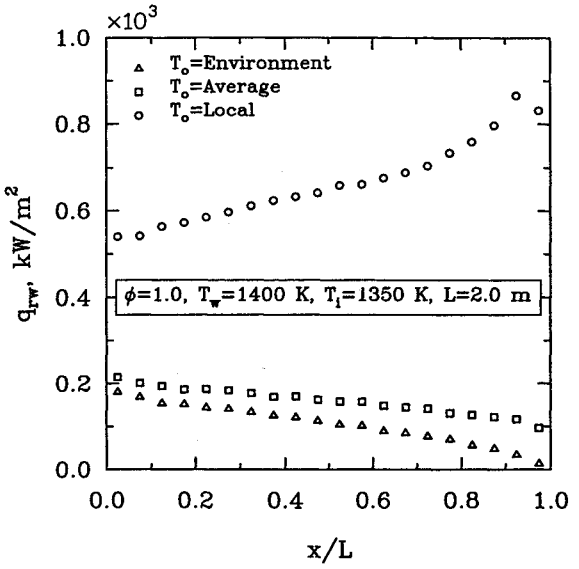


**Fig. 3 Comparison of radiative wall fluxes for different outlet boundary conditions.**

treatment, only surface radiation exchange is taken into account and the results are labeled as nongas in the figures. When radiation is simulated by the gray gas model, radiation absorption and emission are overestimated. In the Monte Carlo simulation an energy bundle travels a shorter distance for the gray gas model than that for the nongray gas model. For the specific case considered in Figs. 4a and 4b, the traveling distance for a typical energy bundle is smaller than $L$ for the gray gas model and is larger than $L$ for the nongray gas model. Consequently, an energy bundle is more likely to be absorbed in the gas in the gray gas treatment and on the wall in the nongray gas treatment. This demonstrates that the radiative source results are positive for the gray gas model and negative for the nongray gas model, whereas the radiative heat fluxes are negative for the gray gas model and positive for the nongray gas model. As far as the nongas model is concerned, since there is no radiation absorption and emission in the gas, the radiative source results are equal to zero; and the radiative wall fluxes are seen to lie between the predictions of the gray gas model and nongray gas model. Comparisons of the results in Figs. 4a and 4b have clearly demonstrated the importance of accurate simulation of radiation. The results of the gray gas model as well as nongas model are obviously not acceptable.

The radiative effects on the nozzle flowfield are negligible. However, these effects are important in assessing the overall heat transfer to the nozzle wall. Under certain conditions, these effects can be significant as compared to the convective heat transfer to the nozzle. Results have been obtained to demonstrate the relative importance of radiative and convective wall fluxes by changing the equivalence ratio, wall temperature, inlet flow temperature, and nozzle size. The convective wall flux is defined in the usual manner as $q_{cw} = -k(T_w)(\partial T/\partial n)_{wall}$, where $n$ represents direction normal to the wall.

The effects of $\phi$ on $q_{rw}$ and $q_{cw}$ are illustrated in Fig. 5. For a specific $\phi$ value, $q_{cw}$ is seen to increase first, reach a peak, and then go down. This is compatible with the trend in temperature variation as seen in Fig. 2a. With the exception of no initial peak, the change in $q_{rw}$ is seen to be similar to that in $q_{cw}$. This is because temperature plays a dominant role in the determination of $q_{rw}$ for the cases considered. Comparing the values of $q_{rw}$ and $q_{cw}$ for each case, it is clear that the radiation is dominant. The results for three different equivalence ratios reveal different behaviors for combustion with lean and rich mixtures. As $\phi$ increases from 0.6 to 1.0, the flow temperature and $H_2O$ mass fraction increase by about 10% and 50%, respectively, and pressure decreases by about 5%. The effects of

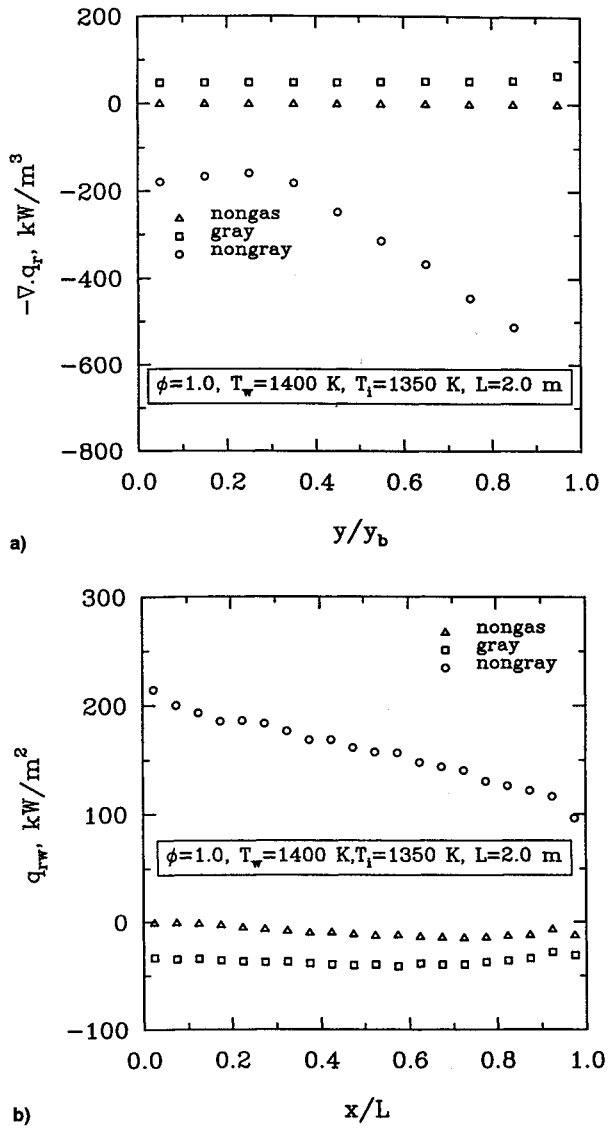


**Fig. 4 a) Comparison of radiative source distributions for nongray gas, gray gas, and nongas models at *X/L* and b) comparison of radiative wall fluxes for nongray gas, gray gas, and nongas models.**

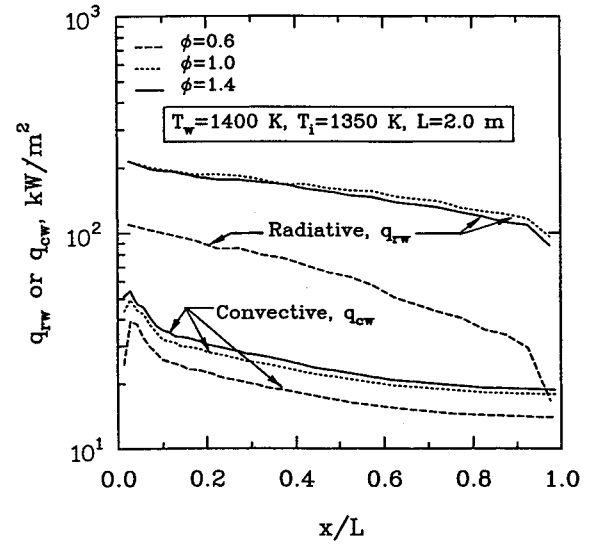


**Fig. 5 Comparison of radiative and convective wall fluxes for three different equivalence ratios.**

these changes result in a sizable increase in the values of $q_{rw}$ and $q_{cw}$. However, as $\phi$ increases from 1.0 to 1.4, the flow pressure decreases by about 10% and $H_2O$ mass fraction increases by about 15%, but the temperature shows little change. This results in only a slight change in the values of $q_{rw}$ and $q_{cw}$.

Figure 6 shows the effects of the nozzle wall temperature on $q_{rw}$ and $q_{cw}$. The change in the nozzle wall temperature is found to have little influence on the combustion. Consequently, the flow temperature, pressure, and $H_2O$ mass fraction remain almost the same in most regions as $T_w$ varies from 1100 to 1700 K. An increase of $T_w$ results in an increase of the absorbed radiant energy on the wall. But this is overshadowed by an increase of the emitted radiant energy from the wall. Since the value of $q_{rw}$ is equal to the absorbed radiant energy minus the emitted radiant energy, the $q_{rw}$ with higher $T_w$ shows a lower value. The trend for $q_{cw}$ is different from $q_{rw}$. As $T_w$ is increased, the temperature gradient near the wall is decreased, but the thermal conductivity for the near wall gas is increased. Since the effect of the thermal conductivity is dominant, $q_{cw}$ is seen to increase with an increase in $T_w$.

The effects of the inlet flow temperature $T_i$ on $q_{rw}$ and $q_{cw}$ are demonstrated in Fig. 7. As $T_i$ varies from 1100 to 1350 K,

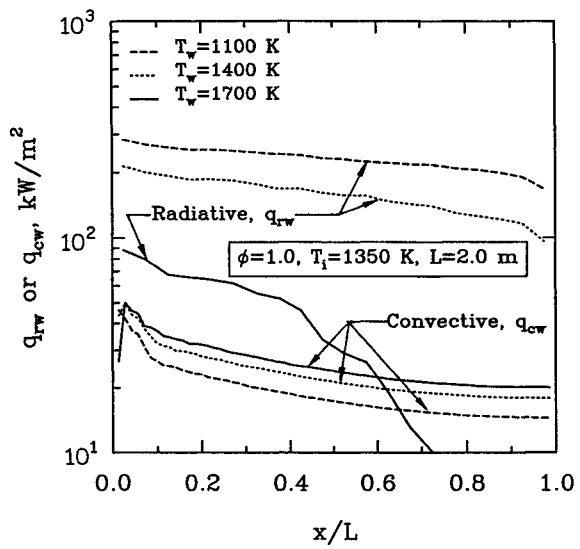


**Fig. 6 Comparison of radiative and convective wall fluxes for three different wall temperatures.**

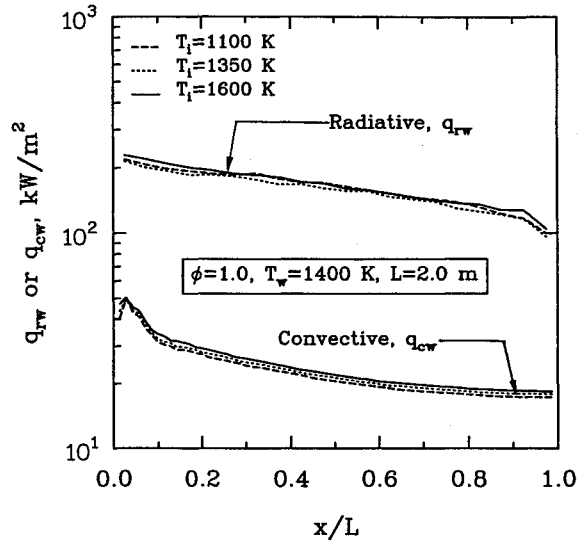


**Fig. 7 Comparison of radiative and convective wall fluxes for three different inlet temperatures.**

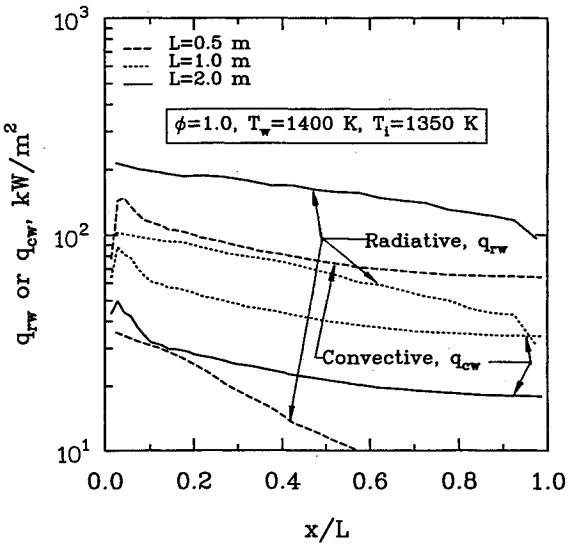


**Fig. 8 Comparison of radiative and convective wall fluxes for three different nozzle sizes.**

the flow temperature increases by about 5% while the pressure and $H_2O$ mass fraction decrease by about 10 and 5%, respectively. A similar trend is noted when $T_i$ varies from 1350 to 1600 K. An increase in temperature tends to reinforce the radiation while a decrease of pressure and $H_2O$ mass fraction tends to reduce the radiation. The combination of these effects results in little change for $q_{rw}$ for different inlet flow temperatures. Similar to $q_{rw}$, $q_{cw}$ is seen to change only slightly with $T_i$ because the temperature gradient near the wall is not changed significantly.

Finally, the effects of the nozzle size on $q_{rw}$ and $q_{cw}$ are illustrated in Fig. 8. By changing the nozzle length, geometrically similar nozzles (with different sizes) can be obtained. As the nozzle length is reduced from 2.0 to 1.0 m and then from 1.0 to 0.5 m, the flow temperature and $H_2O$ mass fraction decrease by about 5%, whereas the pressure increases by about 5% at each stage. The effect of increased pressure on the radiation is overshadowed by a decrease in the nozzle size, temperature, and $H_2O$ mass fraction. Consequently, the lower values of $q_{rw}$ are seen in the figure as the nozzle length is reduced. For the smaller nozzle size, the flow temperature may be lower, but the temperature gradient near the wall is actually higher. Therefore, contrary to $q_{rw}$, the $q_{cw}$ value is seen to increase with a decrease in the nozzle size. The opposite trends in $q_{rw}$ and $q_{cw}$ may yield a tradeoff on the role of radiation in heat transfer on the nozzle wall. With a decrease of nozzle size, the differences between the values of $q_{rw}$ and $q_{cw}$ are reduced and the dominance of radiation is diminished. In fact, for $L = 0.5$, the value of $q_{cw}$ is larger than the value of $q_{rw}$. Therefore, the radiation will become less important and the convection will replace the radiation as dominant mode of heat transfer on the nozzle wall as the nozzle size becomes smaller.

## Conclusions

Radiative heat transfer has been investigated for chemically reacting supersonic flows of premixed hydrogen and air in an expanding nozzle. The MCM has been found to be a very convenient and reliable tool to analyze radiative heat transfer in multidimensional nongray systems. For chemically reacting supersonic flows, the effects of radiation on the flowfield can be neglected, but the radiative effects on the heat transfer to the nozzle wall may be significant. Therefore, accurate simulation of radiation becomes necessary. Extensive parametric studies on the radiative and convective wall fluxes have demonstrated that the magnitude of the radiative and convective wall fluxes are very sensitive to the equivalence ratio when the equivalence ratio is less than 1.0, but they may not be so when the equivalence ratio is higher than 1.0. The change in the wall temperature has little effect on the combustion. The radiative wall flux is decreased, but the convective wall flux is increased with an increase of wall temperature. Inlet flow temperatures have little influence on radiative and convective wall fluxes. The radiative wall flux decreases, but the conductive wall flux increases with a reduction of nozzle size. For large nozzles, the radiative wall flux is dominant over the conductive wall flux. However, the situation may be reversed when the nozzle size is reduced. This information should be useful in proper design of high-speed nozzles.

## Acknowledgments

This work, in part, was supported by the NASA Langley Research Center through Grant NAG-1-363 entitled Institute for Computational and Applied Mechanics (ICAM).

## References

[1]Cess, R. D., Mighdoll, P., and Tiwari, S. N., "Infrared Radiative Heat Transfer in Nongray Gases," *International Journal of Heat and Mass Transfer*, Vol. 10, No. 10, 1967, pp. 1521–1532.

[2]Buckius, R. O., "The Effect of Molecular Gas Absorption on Radiative Heat Transfer with Scattering," *Journal of Heat Transfer*, Vol. 104, Nov. 1982, pp. 580–586.

[3]Edwards, D. K., "Molecular Gas Band Radiation," *Advances in Heat Transfer*, Vol. 12, Academic, New York, 1976.

[4]Soufiani, A., and Taine, J., "Application of Statistical Narrow-Band Model to Coupled Radiation and Convection at High Temperature," *International Journal of Heat and Mass Transfer*, Vol. 30, No. 3, 1987, pp. 437–447.

[5]Zhang, L., Soufiani, A., and Taine, J., "Spectral Correlated and Non-Correlated Radiative Transfer in a Finite Axisymmetric System Containing an Absorbing and Emitting Real Gas-Particle Mixture," *International Journal of Heat and Mass Transfer*, Vol. 31, No. 11, 1988, pp. 2261–2272.

[6]Soufiani, A., Hartmann, J. M., and Taine, J., "Validity of Band-Model Calculation for $CO_2$ and $H_2O$ Applied to Radiative Properties and Conductive-Radiative Transfer," *Journal of Quantitative Spectroscopy and Radiative Transfer*, Vol. 33, No. 3, 1985, pp. 243–257.

[7]Menart, J. A., Lee, H. S., and Kim, T. K., "Discrete Ordinates Solutions of Nongray Radiative Transfer with Diffusely Reflecting Walls," *Journal of Heat Transfer*, Vol. 115, Feb. 1993, pp. 184–193.

[8]Nelson, D. A., "Band Radiation Within Diffuse-Walled Enclosures, Part I: Exact Solutions for Simple Enclosures," *Journal of Heat Transfer*, Vol. 101, Feb. 1979, pp. 81–84.

[9]Nelson, D. A., "Band Radiation Within Diffuse-Walled Enclosures, Part II: An Approximate Method Applied to Simple Enclosures," *Journal of Heat Transfer*, Vol. 101, Feb. 1979, pp. 85–89.

[10]Liu, J., and Tiwari, S. N., "Investigation of Radiative Transfer in Nongray Gases Using a Narrow Band Model and Monte Carlo Simulation," *Journal of Heat Transfer*, Vol. 116, Feb. 1994, pp. 160–166.

[11]Soufiani, A., "Gas Radiation Spectral Correlated Approaches for Industrial Applications," *Heat Transfer in Radiating and Combusting Systems*, edited by M. G. Carvalho, F. Lockwood, and J. Taine, Springer–Verlag, Berlin, 1991.

[12]Mani, M., and Tiwari, S. N., "Investigation of Supersonic Chemically Reacting and Radiating Channel Flow," NASA CR-182726, Jan. 1988.

[13]Tiwari, S. N., Chandrasekhar, R., Thomas, A. M., and Drummond, J. P., "Investigation of Chemically Reacting and Radiating Supersonic Internal Flows," AIAA Paper 91-0572, Jan. 1991.

[14]Suehla, R. A., "Estimated Viscosities and Thermal Conductivities of Gases at High Temperatures," NASA TR R-132, Oct. 1962.

[15]Bird, R. B., Stewart, W. E., and Lightfoot, E. N., *Transport Phenomena*, Wiley, New York, 1960.

[16]McBride, B. J., Heimel, S., Ehlers, J. G., and Gordon, S., "Thermodynamic Properties to 6000 °K for 210 Substances Involving the First 18 Elements," NASA SP-3001, 1963.

[17]Drummond, J. P., Rogers, R. C., and Hussaini, M. Y., "A Detailed Numerical Model of a Supersonic Reacting Mixing Layer," AIAA Paper 86-1427, June 1986.

[18]Cai, J. C., Lee, H. S., and Patankar, S. V., "Treatment of Irregular Geometries Using a Cartesian-Coordinates-Based Discrete-Ordinates Method," *Proceedings of the 29th National Heat Transfer Conference* (Atlanta, GA), American Society of Mechanical Engineers HTD-Vol. 244, 1993, pp. 49–54.

[19]Malkmus, W., "Random Lorentz Band Model with Exponential-Tailed $S^{-1}$ Line-Intensity Distribution Function," *Journal of the Optical Society of America*, Vol. 57, No. 3, 1967, pp. 323–329.
[20]Ludwig, C. B., Malkmus, W., Reardon, J. E., and Thompson, J. A. L., "Handbook of Infrared Radiation from Combustion Gases," NASA SP-3080, Sept. 1973.
[21]Hartmann, J. M., Levi Di Leon, R., and Taine, J., "Line-by-Line and Narrow-Band Statistical Model Calculations for $H_2O$," *Journal of Quantitative Spectroscopy and Radiative Transfer*, Vol. 32, No. 2, 1984, pp. 119–127.
[22]Godson, W. L., "The Evaluation of Infrared Radiation Fluxes Due to Atmospheric Water Vapor," *Quarterly Journal of Royal Meteorological Society*, Vol. 79, No. 341, 1953, pp. 367–379.
[23]Howell, J. R., "Application of Monte Carlo to Heat Transfer Problems," *Advances in Heat Transfer*, Vol. 5, Academic, New York, 1968.
[24]Liu, J., and Tiwari, S. N., "Spectrally Correlated Monte Carlo Formulations for Radiative Transfer in Multi-Dimensional Systems," *Journal of Thermophysics and Heat Transfer*, Vol. 9, No. 2, 1995, pp. 375–378.
[25]Kim, T. K., Menart, J. A., and Lee, H. S., "Nongray Radiative Gas Analyses Using the S-N Discrete Ordinates Method," *Journal of Heat Transfer*, Vol. 113, Nov. 1991, pp. 946–952.
[26]Drummond, J. P., Hussaini, M. Y., and Zang, T. A., "Spectral Methods for Modelling Supersonic Chemically Reacting Flowfields," *AIAA Journal*, Vol. 24, No. 9, 1986, pp. 1461–1467.
[27]Carpenter, M. H., "A Generalized Chemistry Version of SPARK," NASA CR-4196, Nov. 1988.
[28]Siegel, R., and Howell, J. R., *Thermal Radiation Heat Transfer*, 3rd ed., Hemisphere, New York, 1992.